Open
ACCESS

The Presenilin-1 ΔE9 Mutation Results in Reduced γ-Secretase Activity, but Not Total Loss of PS1 Function, in Isogenic Human Stem Cells

Grace Woodruff,[1,4] Jessica E. Young,[1,4] Fernando J. Martinez,[1] Floyd Buen,[1] Athurva Gore,[3] Jennifer Kinaga,[1] Zhe Li,[3] Shauna H. Yuan,[2] Kun Zhang,[3] and Lawrence S.B. Goldstein[1,2,*]

[1]Department of Cellular and Molecular Medicine, Institute for Genomic Medicine and Institute of Engineering in Medicine, University of California, San Diego, La Jolla, CA 92093, USA
[2]Department of Neurosciences, Institute for Genomic Medicine and Institute of Engineering in Medicine, University of California, San Diego, La Jolla, CA 92093, USA
[3]Department of Bioengineering, Institute for Genomic Medicine and Institute of Engineering in Medicine, University of California, San Diego, La Jolla, CA 92093, USA
[4]These authors contributed equally to this work
*Correspondence: lgoldstein@ucsd.edu
http://dx.doi.org/10.1016/j.celrep.2013.10.018

SUMMARY

Presenilin 1 (PS1) is the catalytic core of γ-secretase, which cleaves type 1 transmembrane proteins, including the amyloid precursor protein (APP). PS1 also has γ-secretase-independent functions, and dominant PS1 missense mutations are the most common cause of familial Alzheimer's disease (FAD). Whether PS1 FAD mutations are gain- or loss-of-function remains controversial, primarily because most studies have relied on overexpression in mouse and/or nonneuronal systems. We used isogenic euploid human induced pluripotent stem cell lines to generate and study an allelic series of PS1 mutations, including heterozygous null mutations and homozygous and heterozygous FAD PS1 mutations. Rigorous analysis of this allelic series in differentiated, purified neurons allowed us to resolve this controversy and to conclude that FAD PS1 mutations, expressed at normal levels in the appropriate cell type, impair γ-secretase activity but do not disrupt γ-secretase-independent functions of PS1. Thus, FAD PS1 mutations do not act as simple loss of PS1 function but instead dominantly gain an activity toxic to some, but not all, PS1 functions.

INTRODUCTION

Alzheimer's disease (AD) is a progressive neurodegenerative disease that is the most common cause of dementia (Barnes and Yaffe, 2011). Pathologically, AD is characterized by amyloid plaques consisting of amyloid-beta (Aβ) peptides and neurofibrillary tangles composed of hyperphosphorylated tau protein. Whereas the precise mechanism that causes AD is still under investigation, key proteins involved in the disease have been identified. The amyloid precursor protein (*APP*) and the presenilin genes (*PSEN1* and *PSEN2*) are all implicated in AD because mutations in these genes cause dominantly inherited forms of the disease. Presenilin 1 (PS1) is a multipass transmembrane protein with multiple biological functions. PS1 undergoes proteolytic processing (Thinakaran et al., 1996) to form N- and C-terminal fragments, which then associate with nicastrin, anterior pharynx-defective 1, and presenilin enhancer 2 to form the γ-secretase complex (Edbauer et al., 2003). PS1 functions as the catalytic core of γ-secretase, which cleaves type 1 transmembrane proteins, such as APP, Notch, and cadherins. When APP is cleaved by γ-secretase, the Aβ fragment, a main component of senile plaques, is generated. In addition, PS1 has γ-secretase-independent functions, such as maturation and trafficking of transmembrane proteins, including nicastrin and TrkB (Leem et al., 2002; Naruse et al., 1998), and downregulation of Wnt signaling through destabilization of β-catenin (Killick et al., 2001). More recently, PS1 has also been shown to control lysosome acidification (Lee et al., 2010; Wolfe et al., 2013).

Mutations in PS1 are the most common cause of FAD, with over 100 mutations reported to be pathogenic (http://www.molgen.ua.ac.be/ADMutations; Tanzi and Bertram, 2005). The dominant amyloid cascade hypothesis posits that familial AD (FAD) mutations act by increasing the formation of toxic Aβ fragments of APP, which are generated by sequential cleavage of APP by β-secretase and then by γ-secretase. The most abundant form (∼85%) of the Aβ peptide contains 40 amino acid residues (Aβ40), with a minority (∼15%) of an alternative species containing 42 amino acids, Aβ42. FAD PS1 mutations generally increase the proportion of the Aβ42 peptide, which is thought to be the key agent that causes the pathological changes in FAD (Scheuner et al., 1996). Whether PS1 mutations cause

Table 1. Isogenic iPSC and NPC Lines

Genotype	Number of iPSC Clones[a]	Number of NPC Lines[b]
WT/WT	6	2
WT/null	1	1
WT/Δe9	3	2
Δe9/Δe9	2	2
Δe9/null	2	2

[a]Number of iPSC clones is the total number of clones that received the indicated mutations.
[b]Number of NPC lines is the number of iPSC clones that were used to make NPCs.

increases in Aβ42 and therefore FAD by a gain- or loss-of-function mechanism remains controversial. Controversy persists because virtually all previous studies probing the nature of FAD PS1 mutations have relied on experimental manipulations that overexpress PS1 and PS1 mutants in mouse and/or nonneuronal systems (Bentahir et al., 2006; Chávez-Gutiérrez et al., 2012; Kumar-Singh et al., 2006) or that express mutant forms of PS1 in competition with wild-type forms in cell types that may not have normal levels of expression of other key genes. For example, studies of cultured neurons completely lacking PS1 result in near absence of Aβ generation suggesting that FAD PS1 mutations cause a gain of function (De Strooper et al., 1998). Paradoxically, removal of PS1 from neurons in the adult mouse brain causes neurodegeneration with aspects of neuropathology similar to that seen in AD (Saura et al., 2004). This result led to the suggestion that FAD PS1 mutations generate loss of function of PS1. Similarly, studies using overexpression of PS1 FAD mutations are difficult to interpret, primarily because overexpression of FAD PS1 mutants do not accurately recapitulate normal activity and function of the PS1 protein and because these studies are done in nonneuronal cell types that do not express the same amounts of key PS1-interacting proteins as in neurons. Finally, because mouse models of FAD do not fully recapitulate the pathologies seen in human patients (Games et al., 1995; Radde et al., 2008; Ashe and Zahs, 2010), differences between mouse and human responses to FAD PS1 mutations may be important.

In view of the persistent controversy about the mechanism of dysfunction caused by FAD PS1 mutations, we set out to test whether a key and representative FAD PS1 mutation, PS1 Δe9, expressed at endogenous levels in human neurons and in an isogenic genetic background, is similar to or different from targeted PS1 haploinsufficiency. To achieve this goal, we used induced pluripotent stem cell (iPSC) technology (Takahashi et al., 2007), which provides the opportunity to study bona fide human neuronal cells that express normal levels of neuronal genes, proteins, and pathways. To compare the effects of specific mutations in a controlled isogenic genetic background, we used genome-editing technology with TAL effector nucleases (TALENs) (Miller et al., 2011; Sander et al., 2011) to generate and study an allelic series of PS1 mutations, including the FAD PS1 ΔE9 mutation. This mutation lacks the PS1 endoproteolysis site, thus preventing normal PS1 cleavage during maturation, which facilitates precise quantitative determination of the level

of mutant protein in neuronal cells. We compared the phenotypic consequences of FAD PS1 ΔE9 mutations to heterozygous PS1-null mutations, which enabled us to rigorously conclude that the PS1 ΔE9 mutant acts as a dominant gain-of-function mutation by poisoning intact γ-secretase enzyme complexes in human neuronal cells.

RESULTS

Generation of Isogenic iPSC Lines Carrying Different PS1 Mutations with TALENs

There are several genome-editing methods that have been used to edit iPSCs, zinc finger nucleases (ZFNs) (Soldner et al., 2011), TALENs (Hockemeyer et al., 2011), and more recently the CRISPR/Cas9 system (Mali et al., 2013). We compared both ZFNs and TALENs (Figure S1) and used TALENs for our genome-editing strategy. We designed TALENs to target the PS1 gene in the genome of iPSCs derived from J. Craig Venter (Gore et al., 2011), whose genome has been sequenced and is publicly available (Levy et al., 2007). The FAD PS1 ΔE9 mutation is a point mutation in the splice acceptor consensus sequence of intron 8 that causes in-frame skipping of exon 9 (Perez-Tur et al., 1995). To introduce the ΔE9 point mutation, we used single-stranded oligodeoxynucleotides (ssODNs) (Chen et al., 2011) as the repair template with 60 bp of PS1 homology on either side. We recovered and screened 192 clonal iPSC lines using allele-specific PCR to identify lines that had the ΔE9 mutation. From 192 candidate lines, 14 lines amplified in the allele-specific PCR. We cloned and sequenced the PCR products to test whether candidate lines had incorporated one or two copies of the ΔE9 mutation and whether candidate lines had any disruption of the PS1 gene (i.e., insertions or deletions). This analysis resulted in recovery of an allelic series of PS1 mutations in otherwise isogenic iPSCs (Table 1; Figure 1A). Although our strategy was not designed to detect iPSC lines with disruption of the PS1 locus, we obtained one line with disruption of one PS1 allele (wild-type [WT]/null) caused by insertion of one nucleotide in exon 9. This single-nucleotide insertion interrupts the PS1 open reading frame, causes a premature stop codon, and likely induces nonsense-mediated decay of the PS1 mRNA templated by this allele (Figure 1B). In total, we generated three lines with one copy of the ΔE9 mutation (WT/Δe9), two lines that were homozygous for the ΔE9 mutation (Δe9/Δe9), and two lines with one allele containing the ΔE9 mutation and the other allele an insertion in exon 9 that disrupts the PS1 gene (Δe9/null).

Because γ-secretase activity is key to many developmental pathways (De Strooper et al., 1999), we tested whether introducing the FAD PS1 ΔE9 mutation or disrupting one copy of the PS1 gene affects pluripotency. Staining of iPSC lines with a typical cell-surface pluripotency marker, Tra-1-81, revealed no obvious differences between mutant and control lines (Figure S1F). To test neuronal differentiation, we generated neural progenitor cells (NPCs) from the isogenic iPSCs. Two NPC lines per genotype were generated, with the exception of the WT/null genotype where we only obtained one iPSC line (Table 1). We used the PA6 coculture differentiation protocol previously used in our lab (Yuan et al., 2011) along with dual SMAD inhibition (Chambers et al., 2009) to generate NPCs. After the 12-day

A

```
          GAATTTTGTCTTTCCCAACAGCAACAATGGTGTGGTT          Wild-type PS1
                                                             Sequence
         EcoRI           Δe9=G→T
      5'GAATTCTGTCTTTCCCAACATCAACAATGGTGTGGTT 3'         ssODN
Number of Clones:
      2   GAATTTTGTCTTTCCCAACAGCAACAATGGTGTGGTT          wt/wt
          GAATTTTGTCTTTCCCAACAGCAACAATGGTGTGGTT

      1   GAATTTTGTCTTTCCCAACAGCAA-CAATGGTGTGGTT         wt/1bp Ins
          GAATTTTGTCTTTCCCAACAGCAAACAATGGTGTGGTT

      2   GAATTTTGTCTTTCCCAACAGCAACAATGGTGTGGTT          wt/Δe9
          GAATTCTGTCTTTCCCAACATCAACAATGGTGTGGTT

      2   GAATTTTGTCTTTCCCAACATCAACAATGGTGTGGTT          Δe9/Δe9
          GAATTCTGTCTTTCCCAACATCAACAATGGTGTGGTT

      1   GAATTCTGTCTTTCCCAACATCAACAAT--------GGTGTGGTT   Δe9/7bp Ins
          GAATTTTGTCTTTCCCAACAGCAACAATAATAAAATGGTGTGGTT

      1   GAATTCTGTCTTTCCCAACATCAA-CAATGGTGTGGTT         Δe9/1bp Ins
          GAATTTTGTCTTTCCCAACAGCAAACAATGGTGTGGTT
```


B PS1 mRNA Expression

C

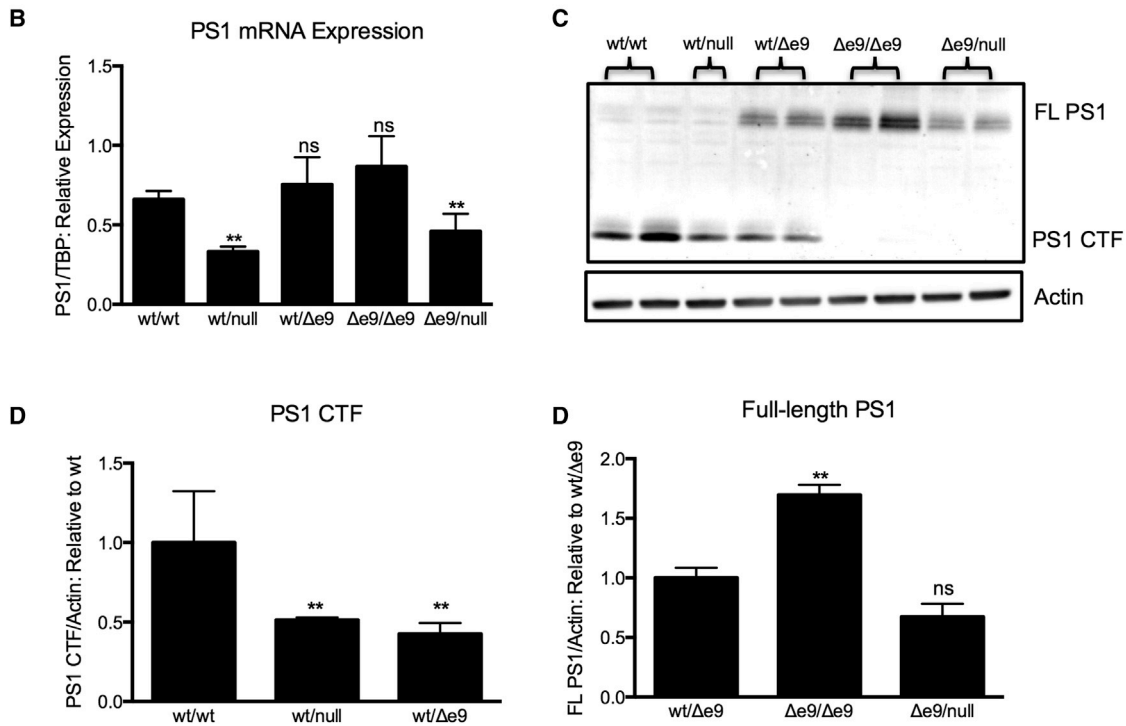**D** PS1 CTF

D Full-length PS1

Figure 1. PS1 mRNA Is Reduced by Null, but Not FAD PS1 ΔE9, Mutations

(A) Generation of isogenic iPSC lines harboring PS1-null and ΔE9 mutations. Insertions of the ΔE9 mutation or random nucleotide insertions that disrupt the PS1 gene are shown for each allele from each line. The wild-type nucleotide is depicted in blue, and mutations or insertions are in red.

(B) PS1 mRNA levels by qPCR from isogenic NPC lines normalized to TBP. The error bars represent SEM from experiments with technical replicates n = 3.

(C) Western blot for PS1 protein from lysates from each NPC line.

(D) Quantification of PS1 CTF with reference to actin and normalized to the levels in the WT/WT lines. Error bars represent SEM from biological replicates n = 2.

(E) Quantification of full-length (FL)-PS1 with reference to actin and normalized to the levels in the WT/Δe9 clones. Error bars represent SEM from biological replicates n = 2.

See also Figure S1.

Table 2. IPSC and hESC Subclones Have a Low Number of Protein-Coding Mutations

Cell Line and Subclone	Unique Mutations[a]	Chromosome	Gene	Protein Change[b]	Mutation Type[c]	Prediction[d]
iPSC-CVB 1.7	0	N/A	N/A	N/A	N/A	N/A
iPSC-CVB 1.8	0	N/A	N/A	N/A	N/A	N/A
iPSC-CVB 1.9	3	2,2,8	ACSL3, CCDC108, DKK4	P129S	nonsyn	tolerated
				V398F	nonsyn	damaging
				C166C	syn	N/A
iPSC-CVI 1.13	0	N/A	N/A	N/A	N/A	N/A
iPSC-CVI 1.14	0	N/A	N/A	N/A	N/A	N/A
iPSC-CVI 1.15	1	2	WDR33	P587S	nonsyn	tolerated
hESC-Hues9 1.7	0	N/A	N/A	N/A	N/A	N/A
hESC-Hues9 1.8	0	N/A	N/A	N/A	N/A	N/A
hESC-Hues9 1.9	1	8	POTEA	M299R	nonsyn	damaging

[a]Number of mutations unique to this cell line compared to the parental iPSC or HUES cell lines.
[b]Indicates whether the detected mutation will change amino acids in the protein.
[c]Indicates whether the mutation is synonymous or nonsynonymous.
[d]Indicates whether the mutation is predicted to be damaging to the protein or tolerated.

differentiation period, we used fluorescence-activated cell sorting (FACS) to purify the NPCs (Yuan et al., 2011) to remove undifferentiated cells and contaminants. We found no significant differences in the percentage of NPCs marked by cell surface markers between the different genotypes (Figure S2A). All NPC lines we recovered exhibited typical morphology and stained positive for the NPC marker, nestin (Figure S3E).

TALEN-Targeted iPSC Lines Harbor Few New Protein-Coding Mutations

Recent studies suggest that reprogrammed iPSC lines can accumulate elevated frequencies of genetic and epigenetic changes potentially owing to reprogramming and subsequent selection during culture and expansion (Hussein et al., 2011; Gore et al., 2011; Lister et al., 2011). Similarly, a concern with using genome-editing strategies, such as TALENs or ZFNs, is the occurrence of off-target effects, in particular double-stranded breaks (DSBs), which may generate insertions or deletions in protein-coding regions other than those intended for targeting. Because targeted iPSCs were subcloned after genome-editing with the TALENs in order to generate clonal cell lines, detecting mutations due to off-target genome editing is complicated by the potential mutational effects of the subcloning process itself.

To address these concerns, we performed whole-exome sequencing on our TALEN-modified iPSC lines and the parent iPSC line and compared the resultant mutational load to that found between nonmodified iPSC subclones and human embryonic stem cell (hESC) subclones and their iPSC and hESC parent population. We generated three single-cell subcloned lines each for two iPSC lines (CVB and CVI) and one hESC line (Hues 9). We analyzed the mutational load of the protein-coding regions of the genome by performing exome sequencing on these nine subcloned lines, the six TALEN-edited lines, and the parent iPSC and hESC lines. We observed a very low frequency of protein-coding mutations (zero to three) in each of the subcloned lines. Additionally, the number of acquired mutations did not differ between the iPSC and hESC lines. The mutational load found in each of the nonmodified iPSC and hESC subclones (Table 2) when

compared to their mixed parent population was statistically very similar to the mutational load found in the TALEN-edited subclones (Table 3) when compared to their mixed parent population (p = 0.13), indicating that TALEN-based genome editing does not introduce an additional point mutational load over subcloning. Additionally, the edited subclones did not possess a detectable increase in indel count, indicating that insertions and deletions due to off-target DSBs did not seem to occur. Furthermore, the edited subclones did not possess any chromosome-level shifts in allele ratios at known SNP sites, indicating that the edited lines are not aneuploid. Taken together, these findings have led us to conclude that subcloning of iPSCs is not inherently highly mutagenic and that modification with TALENs is unlikely to cause any significant off-target effects.

Interestingly, recent work from Ding et al. (2013) reports TALEN modification of Hues1 hESCs. In this paper, TALEN-modified subclones also demonstrated a low number of off-target effects as analyzed by whole-exome and whole-genome sequencing. However, across the subclones, this group found 24 single-nucleotide variants in coding regions, approximately ten times more than we found in our experiment. The reason for this difference is puzzling but could possibly be due to differences in the number of passages the clones underwent prior to subcloning, differences in the maintenance of the cells (i.e., feeders versus feeder-free conditions), or differences inherent to the particular cell line used. One possibility to circumvent this discrepancy and ensure truly isogenic cell lines would be to first subclone iPSCs or hESCs prior to genome-editing with TALENs.

PS1 mRNA Is Substantially Reduced by Null, but Not FAD ΔE9 PS1, Mutations

To test whether the TALEN-induced mutations had the expected molecular effects on PS1 mRNA abundance, we harvested RNA from NPCs of each PS1 genotype and performed quantitative RT-PCR analysis. We found that the WT/null line exhibited decreased PS1 mRNA to ~50% of normal (Figure 1B), which confirmed that the nucleotide insertion in exon 9 results in the

Table 3. TALEN-Targeted iPSC Lines Have a Low Number of Off-Target Mutations

Genotype	Unique Mutations[a]	Chromosome	Gene	Protein Change[b]	Mutation Type[c]	Prediction[d]
WT/WT	0	N/A	N/A	N/A	N/A	N/A
WT/Δe9	1	8	CSMD1	I2038I	syn	tolerated
WT/Δe9	3	4,14,19	SYNE2	E795E	syn	tolerated
			ZNF225	V4668I	nonsyn	tolerated
			PDIA3	G466V	nonsyn	damaging
Δe9/Δe9	1	17	STAT3	R278H	nonsyn	tolerated
Δe9/Δe9	2	5	NUP155	S58Y	nonsyn	tolerated
			PCDH-GA10	A606S	nonsyn	tolerated
Δe9/Δe9	2	5	PCDH-GA10	A606S	nonsyn	tolerated
Δe9/null	1	15	PDIA3	S169S	syn	tolerated

[a]Number of mutations unique to this cell line compared to the parental iPSC or HUES cell lines.
[b]Indicates whether the detected mutation will change amino acids in the protein.
[c]Indicates whether the mutation is a synonymous or nonsynonymous mutation.
[d]Indicates whether the mutation is predicted to be damaging to the protein or tolerated.

loss of PS1 mRNA, likely due to nonsense-mediated decay of the PS1 message. We also observed that the WT/ΔE9 lines and the ΔE9/ΔE9 lines did not significantly differ from WT/WT lines for PS1 mRNA, whereas ΔE9/null had ∼50% of normal levels of PS1 mRNA (Figure 1B). To evaluate PS1 mutant effects on PS1 protein abundance, we took advantage of the finding that PS1 undergoes endoproteolysis to generate a 26 to 27 kDa N-terminal fragment and a 16 to 17 kDa C-terminal fragment (Thinakaran et al., 1996). Part of the endoproteolysis site is in exon 9 of PS1, and thus, an important feature of the ΔE9 mutation is that the endoproteolysis site is destroyed. Therefore, lines containing one copy of ΔE9 are predicted to generate 50% of the cleaved product and 50% of the full-length (∼44 kDa), whereas cells containing two copies of ΔE9 should not generate any of the cleaved product. Western blot analysis using a C-terminal antibody (Figures 2C–2E) revealed that these lines all behaved as predicted with WT/ΔE9 producing 50% of the uncleaved fragment, ΔE9/ΔE9 producing 100% of the uncleaved fragment, and ΔE9/null producing only uncleaved fragment but at 50% the level of ΔE9/ΔE9. To further confirm that the null mutations were indeed a true null allele and not a truncated protein with residual function, we also performed a western blot with an N-terminal antibody (Figures S1G–S1I). Using an N-terminal antibody, we also observed significantly decreased protein from cell lines harboring null PS1 alleles. Thus, based on PS1 mRNA and protein production, we concluded that PS1 mutants induced in isogenic iPSC lines generated the expected effects on PS1 mRNA expression, protein production, and endoproteolysis.

The PS1 ΔE9 Mutation Increases the Aβ42/Aβ40 Ratio in Human Neurons by Decreasing Aβ40

APP normally undergoes several proteolytic processing events to generate a collection of soluble APP fragments, including the APP intracellular domain and Aβ peptides. Aβ peptides are generated when APP first undergoes cleavage by β-secretase and then by cleavage with γ-secretase. FAD mutations in APP, PS1, and PS2 have been shown to alter processing of Aβ, with most mutations reported to increase the Aβ42/Aβ40 ratio when expressed under a variety of conditions (Qiang et al., 2011; Kumar-Singh et al., 2006). Because APP processing in human neurons that generate Aβ peptides, in particular Aβ42, plays a key role in AD pathogenesis, we tested for changes in APP processing in purified human neurons generated from isogenic human NPC lines with different PS1 mutations. Purified neurons were generated by differentiating NPCs for 3 weeks followed by FACS purification (Yuan et al., 2011). We found no significant differences in the percentage of neurons generated between the different genotypes (Figure S2B). We used a highly sensitive assay (Israel et al., 2012) to measure Aβ38, Aβ40, and Aβ42 species from purified cells and progenitors. We found that cell lines harboring one copy of ΔE9 significantly increased the secreted Aβ42/Aβ40 ratio by 2-fold, compared to the WT/WT lines (Figures 2A and 2B). Two copies of ΔE9 increased the Aβ42/Aβ40 ratio 3-fold over WT/WT lines, and similarly, ΔE9/null lines also tripled the Aβ42/Aβ40 ratio over WT/WT. Interestingly, WT/null was not significantly different from WT/WT, demonstrating that loss of one copy of PS1 does not mimic the ΔE9 mutation.

We used purified neurons to investigate whether the ΔE9 mutation increases the Aβ42/Aβ40 ratio by decreasing Aβ40, increasing Aβ42, or both. We observed that the WT/null genotype was not significantly different from WT/WT for Aβ40 (Figure 2C). However, all genotypes containing even a single copy of Δe9, WT/Δe9, Δe9/Δe9, and Δe9/null, had significantly decreased Aβ40 (Figure 2C). There were no significant differences between WT/null and WT/Δe9 in the amount of Aβ42; however, Δe9/Δe9 and Δe9/null genotypes displayed significantly increased amounts of Aβ42 (Figure 2D). Therefore, we conclude that PS1 ΔE9, expressed at endogenous levels in human neurons, increases the Aβ42/Aβ40 ratio by decreasing Aβ40 and increasing Aβ42. Additionally, we determined that loss of one PS1 allele does not significantly alter Aβ production and in particular did not affect the Aβ42/Aβ40 ratio.

Finally, to test whether PS1 ΔE9 affects tau phosphorylation, the other major pathological hallmark of AD, we measured phosphotau at site Thr231, a site that correlates with neurofibrillary tangle number (Buerger et al., 2006). We did not observe any significant differences in the ratio of P-tau/T-tau between any of the PS1 genotypes (Figure S2D).
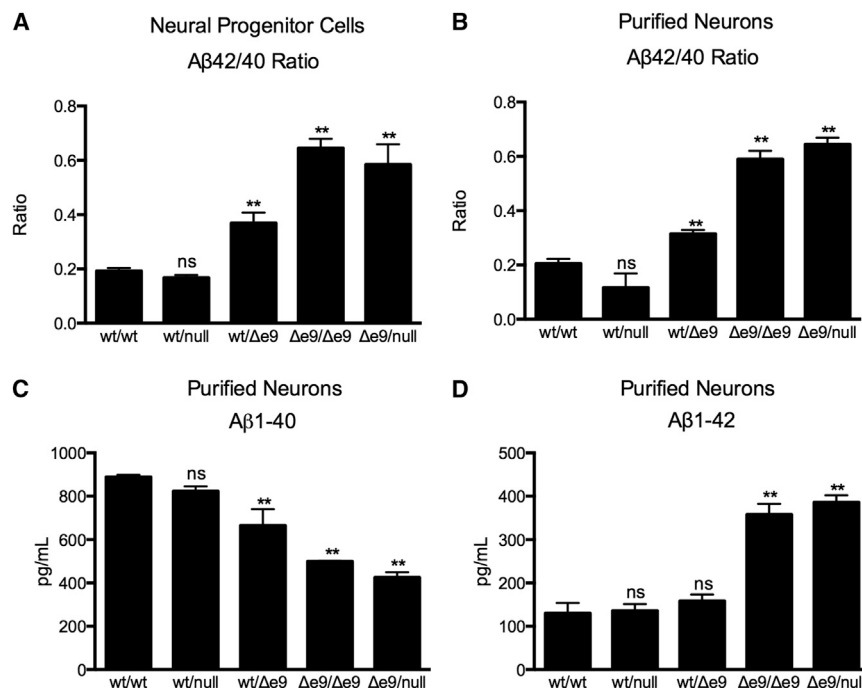
Figure 2. The PS1 Δe9 Mutation Increases the Aβ42/Aβ40 Ratio by Decreasing Aβ40

(A) Secreted Aβ42/Aβ40 ratio from NPCs. Bars represent measurements from two NPC lines per genotype with the exception of the WT/null genotype. Error bars represent SEM from six biological replicates per line.

(B) Secreted Aβ42/Aβ40 ratio from purified neurons. Bars represent measurements from two lines per genotype with the exception of the WT/null genotype. Error bars represent SEM from six biological replicates per line.

(C) Secreted Aβ40 from purified neurons. Error bars represent SEM from six biological replicates per line.

(D) Secreted Aβ42 from purified neurons. Error bars represent SEM from six biological replicates per line.

See also Figure S2.

itor (200 nM) completely inhibits all Aβ production (data not shown) in all genotypes. Strikingly, a low dose (5 nM) of compound E substantially increases the Aβ42/Aβ40 ratio in WT/WT, WT/null, and WT/ΔE9 neurons, but not in ΔE9/ΔE9 or ΔE9/null (Figure 3D). Thus, the ΔE9 muta-

tion has a similar phenotypic impact on Aβ processing as direct and low-level inhibition of γ-secretase. Surprisingly, the ΔE9 mutation appears to confer resistance to low-dose inhibition of γ-secretase activity by compound E.

The PS1 ΔE9 Mutation Impairs γ-Secretase-Dependent Functions of PS1

To determine directly whether the ΔE9 mutation impairs γ-secretase-mediated processing of different protein substrates, we measured the cleavage of the C-terminal fragments (CTFs) of APP and N-cadherin, both of which are γ-secretase substrates. Ordinarily, APP first undergoes cleavage by α and β secretases, which yield α and β CTFs, and then γ-secretase further cleaves the α and β CTFs. Similarly, N-cadherin undergoes an initial proteolytic processing event, which generates a CTF that is also cleaved by γ-secretase. Therefore, if the ΔE9 mutation impairs γ-secretase activity, we would expect to see an increase in APP and N-cadherin CTFs. All lines containing at least one copy of ΔE9 had significantly increased APP CTFs over WT/WT (Figures 3A and 3B). We also quantified full-length APP and observed no significant differences between genotypes (Figure S2A). This suggests that the ΔE9 mutation does impair γ-secretase cleavage of APP CTFs. Similarly, we were unable to detect any N-cadherin CTF for WT/WT, WT/null, and WT/ΔE9 genotypes but did observe obviously elevated levels of CTFs in Δe9/Δe9 lines and Δe9/null lines (Figure 3C). Collectively, these data demonstrate that the ΔE9 mutation expressed at endogenous levels in a normal genetic background in human neurons impairs γ-secretase activity.

Previous studies reported that low doses of γ-secretase inhibitors that moderately impaired γ-secretase function increase the Aβ42/Aβ40 ratio in a variety of cell types (Sato et al., 2003; Shen and Kelleher, 2007). Thus, as an additional test of whether the ΔE9 mutation decreases γ-secretase activity in purified euploid human neurons, we compared the effects of the ΔE9 mutation to a low dose of the γ-secretase inhibitor, compound E. Similar to previous reports, we found that a high dose of γ-secretase inhib-

The PS1 ΔE9 Mutation Does Not Impair γ-Secretase-Independent Functions of PS1

To further probe whether the ΔE9 mutation acts as a loss or gain of function, we asked whether the ΔE9 mutation interferes with a γ-secretase-independent function of PS1, nicastrin maturation. Wild-type PS1 has been reported to facilitate nicastrin maturation by acting as a chaperone in early biosynthetic compartments (Leem et al., 2002). Thus, we quantified the relative amounts of mature and immature nicastrin in purified neurons with various PS1 genotypes by quantitative western blot (Figures 4A and 4B). We found that the ratio of mature/immature nicastrin was significantly decreased compared to WT/WT only in cell lines that harbor a PS1-null mutation (WT/null and Δe9/null). There were no significant differences in mature/immature nicastrin between WT/WT, WT/Δe9, and Δe9/Δe9 genotypes. This result suggests that the ΔE9 mutation does not impair all γ-secretase-independent functions of PS1 because it generates a phenotypic effect that is clearly different from a null allele (Figure 4C).

DISCUSSION

Based on direct quantitative biochemical comparisons, our results demonstrate that the phenotypic effects of a proven null PS1 mutation and an FAD PS1 ΔE9 mutation are not equivalent in isogenic euploid-purified human neurons. In addition, the ΔE9 allele inhibits aspects of γ-secretase activity while maintaining
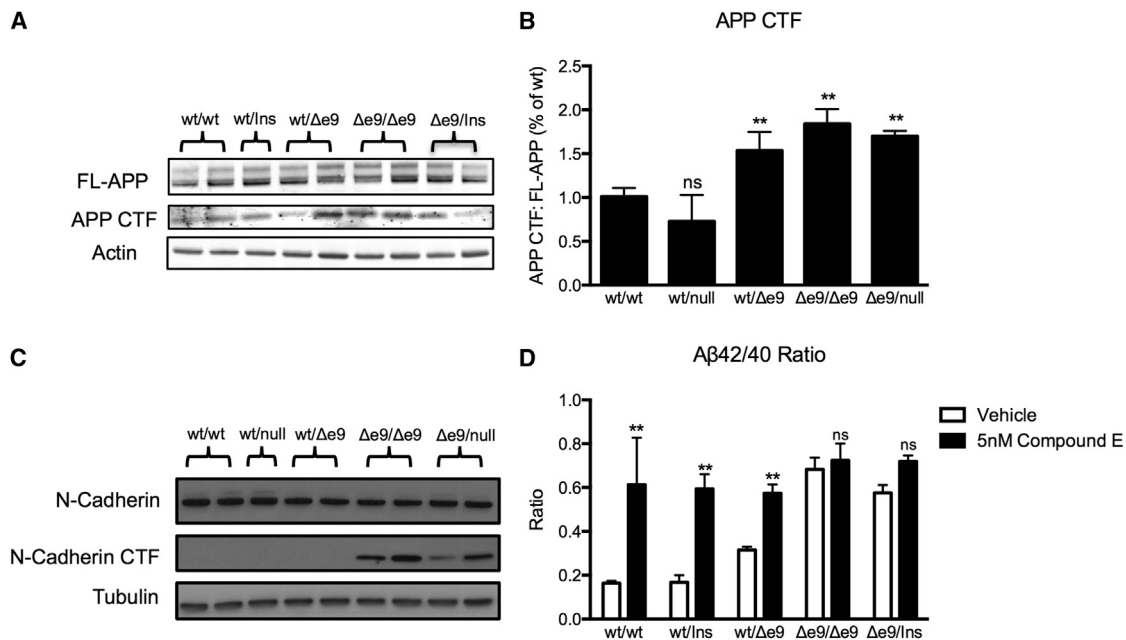
Figure 3. The PS1 ΔE9 Mutation Impairs γ-Secretase Activity
(A) Representative western blot of FL-APP and APP CTF.
(B) Quantification of APP CTF with reference to FL-APP and normalized to levels in WT/WT. Each bar represents measurements from three biological replicates. Error bars represent SEM from three measurements per line.
(C) Western blot of FL N-cadherin and N-cadherin CTF.
(D) Secreted Aβ42/Aβ40 ratio from purified neurons treated with a γ-secretase inhibitor, compound E, at 5 nM. Error bars represent SEM from four biological replicates per line.
See also Figure S2.

normal activity for at least one γ-secretase-independent function, nicastrin maturation. Thus, by using carefully genetically engineered human cells, this series of experiments reveals that some, and we propose by extension, all PS1 FAD mutations are not simple loss-of-function alleles with respect to the biochemical pathway that generates key phenotypes associated with the initiation and development of AD.

Previous experiments probing whether the PS1 ΔE9 mutation changes the Aβ42/Aβ40 ratio by increasing Aβ42, decreasing Aβ40, or both have been reported multiple times with contradictory results (Chávez-Gutiérrez et al., 2012; Kumar-Singh et al., 2006). This issue is important because determining how the FAD PS1 ΔE9 mutation changes the ratio of Aβ species in euploid human neurons may help to elucidate AD mechanisms and inform development of effective AD drugs. By taking advantage of the allelic series we generated in a controlled genetic background in purified human neurons, we were able to determine that the ΔE9 mutation increases the Aβ42/Aβ40 ratio in a gene-dosage-dependent manner by significantly decreasing the amount of Aβ40 while moderately increasing the amount of Aβ42. Our results are in contrast to some, but not all, previous attempts to clarify this issue. For example, a number of previous analyses of FAD PS1 mutations used mouse embryonic fibroblasts (MEFs) or human embryonic kidney (HEK) cells overexpressing PS1 ΔE9; some experiments incorporated additional overexpression of human APP and APP mutations. These

studies are complex to interpret because it is unknown whether overexpression of PS1 ΔE9 results in biochemical data accurately representing the normal activity of PS1. An alternative approach is defined by early studies in *C. elegans*, which suggested that FAD PS1 mutations encode PS1 proteins with decreased activity compared to WT PS1 (Shen et al., 1997). Early studies in HEK cells treated with antisense PS1 RNA showed increased secretion of Aβ42 (Refolo et al., 1999), which also supported the idea that PS1 mutations are simple loss-of-function. Later studies from knockout mice suggested that PS1 mutations are gain-of-function because complete loss of PS1 resulted in severely decreased overall Aβ production, unlike PS1 mutations. More recent studies propose that many PS1 mutations have decreased γ-secretase activity (Bentahir et al., 2006; Koch et al., 2012; Heilig et al., 2010). A common issue among these studies is that evaluation of Aβ production in nonhuman and/or nonneuronal cells may not be ideal because Aβ production and factors influencing Aβ production vary significantly among cell types (Qiang et al., 2011; Israel et al., 2012) and in comparison to neurons, which are the primary cell type affected in AD. Although these differences among cell types and systems might not have large-scale effects, AD itself and AD phenotypes can be generated by relatively minor changes in expression of key genes, e.g., a 50% dosage increase of APP itself is sufficient to generate severe early onset FAD (Rovelet-Lecrux et al., 2006). Our system using genetically manipulated isogenic
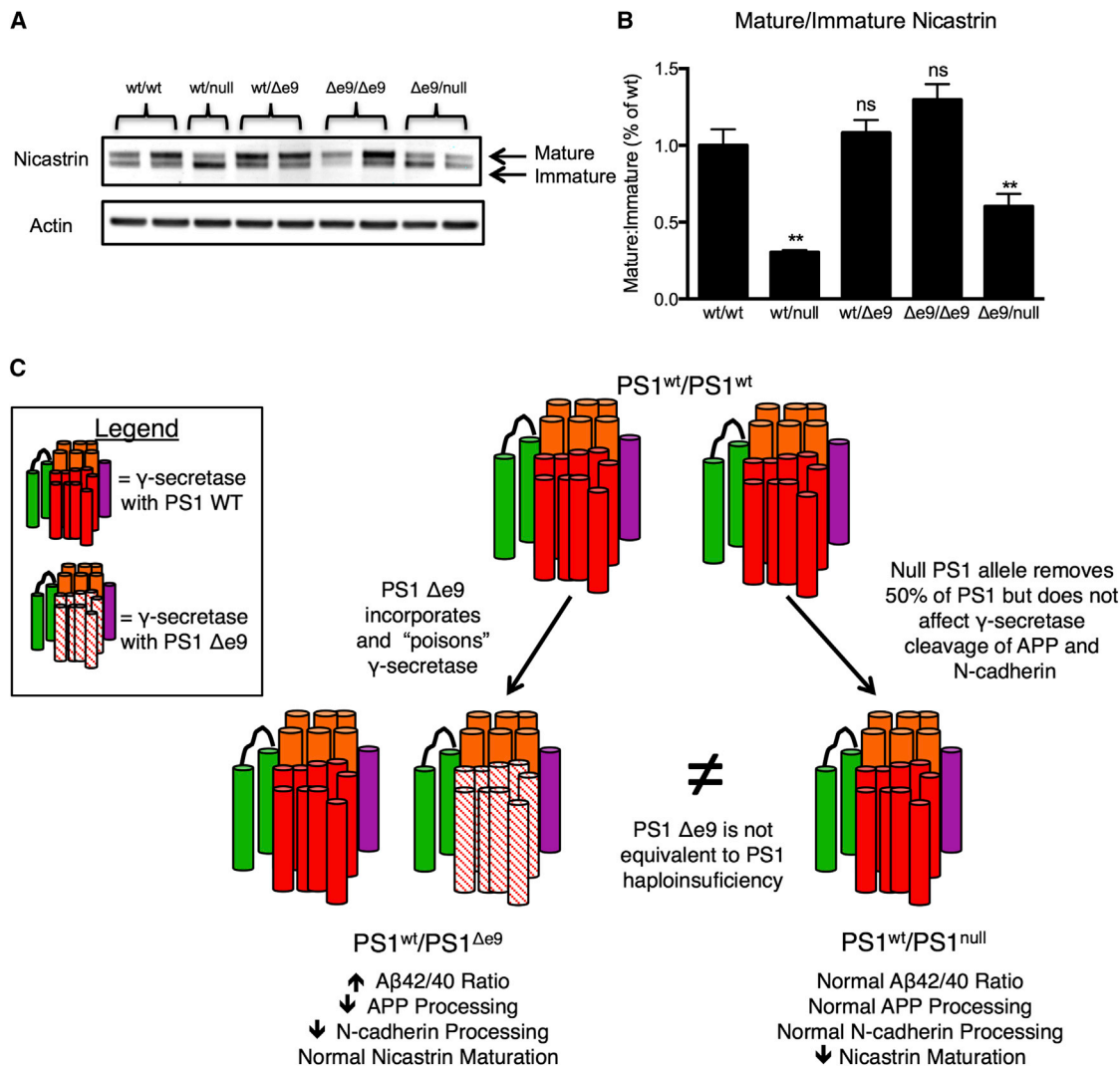
A

B

Mature/Immature Nicastrin

C

Figure 4. PS1-Null Mutations, but Not the PS1 Δe9 Mutation, Impair Nicastrin Maturation
(A) Representative western blot of nicastrin from isogenic lines. Black arrows indicate mature and immature forms of the protein.
(B) Quantification of mature and immature nicastrin. Error bars represent SEM of two biological replicates per line.
(C) Schematic summary of results.

iPSC-derived neurons avoids these problems, allows effects of relatively minor magnitude to be evaluated, and, in principle, avoids problems of uncontrolled dosage at other key loci.

Here, we report a complete and direct comparison of γ-secretase-dependent and -independent functions generated by an FAD PS1 mutation and a null allele. Strikingly, PS1 haploinsufficiency had no significant effect on the Aβ42/Aβ40 ratio or total levels of Aβ40 and Aβ42, which again demonstrates that PS1 loss of function and PS1 ΔE9 are not equivalent with respect to Aβ production and CTF processing. Thus, our finding confirms that the ΔE9 mutation is not simply a complete loss of PS1 function because the ΔE9 mutation has decreased γ-secretase activity compared to WT PS1 and heterozygous null allele but has no effect on nicastrin maturation, a γ-secretase-independent function of PS1. In fact, we found impaired nicastrin maturation

only in cell lines that harbored a PS1-null mutation, which further confirms that PS1 ΔE9 maintains at least some normal PS1 functions. Furthermore, we found that PS1 haploinsufficiency had no detectable effect on APP or N-cadherin cleavage, again suggesting that PS1 haploinsufficiency and PS1 ΔE9 do not have the same effect on γ-secretase activity. Our findings also suggest that, under the physiological conditions of our studies and with respect to the phenotypes measured, γ-secretase activity is available in excess, because loss of one PS1 allele did not significantly alter γ-secretase cleavage of APP or N-cadherin.

In addition to testing how total levels of Aβ and the Aβ42/Aβ40 ratio responded to different PS1 genotypes, we also measured phosphorylation of tau at Thr231. We did not observe any significant differences in the ratio of tau phosphorylated at Thr231 relative to total tau when any of our PS1 mutants or combinations

were compared to WT PS1, even in cell lines that were homozygous for the ΔE9 mutation and had significantly increased Aβ42. This result is similar to recent studies of neurons made from IPSCs carrying two different presenilin mutants, PS1 A246E and PS2 N141I (Yagi et al., 2011) but is in contrast to previous studies of iPSC-derived neurons from FAD caused by an APP duplication (Israel et al., 2012) or trisomy 21 (Shi et al., 2012), both of which reported an increase in the ratio of phosphorylated tau relative to total tau. An intriguing possibility is that FAD caused by an extra copy of APP and FAD caused by PS1 mutations differ in the earliest phenotypes and mechanisms by which they cause disease and thus differ in their induction of abnormal levels of phosphotau. In this context, there is evidence that different FAD mutations result in positional and temporal differences in tau phosphorylation and accumulation. Specifically, analyses of postmortem AD tissue revealed that different PS1 mutations (Shepherd et al., 2004) affect tau deposition and phosphorylation differentially with mutations in PS1 exons 8 and 9 having less hyperphosphorylated tau than mutations in exons 5 and 6. Further studies in iPSC-derived neurons, either with genome modifications or derived from patients with specific FAD mutations, will clarify the nature of tau phenotypes in different FAD mutants.

A major focus of AD therapeutics has been γ-secretase inhibition, which has thus far failed to perform as hoped in clinical trials (Opar, 2008). In some cases, γ-secretase inhibition has even accelerated cognitive decline (Extance, 2010). Our data suggest that γ-secretase inhibition could worsen patients either by increasing the proportion of Aβ42 or by increasing the amount of APP CTFs, which have been proposed to play a role in AD pathogenesis (Rodrigues et al., 2012; Jiang et al., 2010). Interestingly, our recent work in an iPSC-derived human neuronal system (Israel et al., 2012) suggested that the β-CTF of APP is toxic in purified FAD neurons because treatment with a β-secretase inhibitor, rather than a γ-secretase inhibitor, reduced abnormal phosphotau levels in these FAD neurons. Given that the FAD PS1 ΔE9 mutation decreases the amount of Aβ40 in our system and increases the APP CTFs, it is possible that this class of FAD mutation confers its toxic properties, in part, by the accumulation of other pathogenic APP fragments, such as the APP CTF. Thus, a potentially important therapeutic implication from our work is that γ-secretase modulation that restores the Aβ ratios and/or restores γ-secretase function to normal levels or character could be more beneficial for AD treatment. Future studies characterizing other PS1 functions that may be affected by drugs and mutations will also be important for designing AD therapeutics.

A final important implication emerging from the work we report here concerns the question of whether TALENs introduce significant off-target mutations in iPSCs. By performing exome sequencing on genome-edited and subcloned iPSC lines, we found that the genome-edited lines did not have a significantly higher number of unique mutations beyond what we observed in simple iPSC or hESC subcloning experiments. Thus, the introduction of TALENs does not appear to cause major off-target mutagenic effects. Another recent publication (Ding et al., 2013) reported that exome and whole-genome sequencing on TALEN-targeted hESC lines revealed mutations unique to different subclones, although at an apparently higher frequency

than we report here, possibly due to inherent differences in the particular cell line used or in the number of passages the clones underwent prior to subcloning. Altogether, these data suggest that it may be impossible to derive completely isogenic cell lines. However, the relative number of single-nucleotide variants between TALEN-targeted lines is still apparently less than what would be observed between different individual human genomes. Finally, as we report here, the generation of an allelic series and the analysis of multiple independent lines allows for careful evaluation of phenotypic effects in a bona fide, euploid cell-type-representative human model.

EXPERIMENTAL PROCEDURES

iPSC Culture

iPSCs were generated as previously described (Gore et al., 2011; Israel et al., 2012) following informed consent and Institutional Review Board approval. iPSCs are cultured on an irradiated MEF feeder layer generated in-house. Cells are grown in medium containing knockout (KO) Dulbecco's modified Eagle's medium (DMEM) (Gibco), 10% plasmanate (Talecris Biotherapeutics), 10% KO Serum Replacement (Gibco), 20 mM GlutaMax (Invitrogen), 20 mM nonessential amino acids (Invitrogen), 20 mM Pen/Strep (Invitrogen), and 20 ng/ml fibroblast growth factor (FGF) (Millipore). Cells were passaged by dissociation with Accutase (Innovative Cell Technologies).

Isogenic iPSC Generation

iPSCs were pretreated with 10 μM Rock Inhibitor (Ascent Scientific) for 1 hr prior to nucleofection. Cells were dissociated using Accutase and passed through a 100 μM filter to obtain single cells. Two million iPSCs were nucleofected using Amaxa Human Stem Cell Nucleofector Kit 1 (Lonza), with 7.5 μg of each TALEN-encoding plasmid, 2 μg of pmaxGFP (Lonza), and 30 μg of ssODN (Integrated DNA Technologies). Cells were maintained in iPSC culture conditions with 10 μM Rock Inhibitor for 72 hr followed by FACS sorting (FACS Aria; BD Biosciences) for GFP+ cells. GFP-expressing cells were plated at 1 × 10^4 cells per 10 cm plate in the presence of Rock Inhibitor. Thereafter, media was changed every other day until isolated colonies grew. Isolated colonies were manually picked and grown in 96-well plates. Once cells were confluent, cells were split into a duplicate well and grown until confluent, at which point they were harvested for DNA using DNA QuickExtract (Epicenter). DNA was amplified using allele-specific primers to detect the ΔE9 point mutation using Jump Start PCR Ready Mix (Sigma). Cell lines that amplified using the allele-specific PCR were then digested with EcoRI to further confirm insertion of the ssODN. To sequence the PCR products, we cloned them using the Zero Blunt PCR Cloning Kit (Invitrogen).

Exome Sequencing

Exome sequencing was performed as previously described (Gore et al., 2011). Briefly, genomic DNA from each sample was sheared and ligated to barcoded Illumina sequencing adaptors. DNA was then hybridized using the Roche NimbleGen SeqCap EZ Exome library to capture exomic regions. Exome regions were captured with streptavidin-coated beads and then PCR-amplified with Illumina sequencing adaptors. The resulting libraries were sequenced on an Illumina Genome Analyzer IIx or Illumina Hiseq. Reads were mapped to the whole genome using Burrows-Wheeler Alignment tool, and a consensus sequence was generated using the Genome Analysis Toolkit (Broad Institute best practices). Consensus sequences between the progenitor cell lines and subcloned cell lines were compared in order to look for candidate novel mutations. Candidate variants that occurred at locations present in the Single Nucleotide Polymorphism Database or that showed any presence in the progenitor line were removed. Identified candidate mutations were validated by Sanger sequencing.

Statistical Analysis of Mutation Counts

To determine if TALEN modification resulted in an increased off-target point mutational load, the number of mutations in the TALEN-modified subcloned

iPSC lines was compared to the number of mutations in the unmodified subcloned pluripotent stem cell lines. In order to analyze the potential mutational load introduced by the TALEN process itself and exclude any normal culture mutations, the number of mutations acquired after subcloning was analyzed rather than any overall iPSC mutations acquired due to reprogramming or postreprogramming culture. Because of the varied culture history of each progenitor line and subclone, it was difficult to construct a hypothetical mutational distribution for each line. Thus, the nonparametric Mann-Whitney test was used to compare the median number of mutations in each subclone group. The test revealed that TALEN-modified and unmodified subclones had a similar median number of mutations; no significant difference could be determined (p = 0.13). This indicates that TALEN-modified lines do not acquire any additional mutational load over that expected during normal culture and subcloning.

NPC Differentiation, Purification, and Culture

iPSCs were differentiated to NPCs as previously described (Yuan et al., 2011). Briefly, 1×10^5 iPSCs were seeded onto PA6 cells in PA6 differentiation medium: Glasgow DMEM, 10% knockout serum replacement, 1 mM sodium pyruvate, 0.1 mM nonessential amino acids, and 0.1 mM β-mercaptoethanol (all from Invitrogen). For the first 6 days, media was not changed and also contained 500 ng/ml Noggin (R&D Systems) and 10 μM SB431542 (Tocris Bioscience). After the first 6 days, medium was changed every other day until day 12. On day 12, cells were dissociated and stained with CD184, CD44, CD271, and CD24 (all from BD Biosciences). CD184+, CD24+, CD44−, CD271− cells were sorted (FACSAria, BD Biosciences). NPC cultures were cultured on 20 μg/ml poly-L-ornithine- and 5 μg/ml laminin-coated (both from Sigma) plates in medium containing: DMEM:F12 + Glutamax, 0.5× N2, 0.5× B27 (both from Life Technologies), 1× penicillin/streptomycin, and 20 ng/ml FGF (Millipore). Media was changed every other day.

Neuron Differentiation, Purification, and Culture

NPCs were expanded to 10 cm plates and grown to confluency (3 to 4 days), at which point FGF was removed from the media. The medium was changed twice per week, and the cells were differentiated for 21 days. After the 3-week differentiation, neurons were purified as previously described (Yuan et al., 2011). Briefly, cells were dissociated using Accutase and Accumax (both from Innovative Cell Technologies) and then stained with CD184, CD44, and CD24 (all from BD Biosciences). CD184−, CD44−, CD24+ cells were sorted (FACSAria; BD Biosciences) and then plated on poly-ornithine/laminin-coated plates in NPC media + 0.5 mM dbCAMP (Sigma), 20 ng/μl brain-derived neurotrophic factor, and 20 ng/μl glial cell line-derived neurotrophic factor (both from Peprotech).

Gene Expression Analysis

For mRNA expression analysis, total RNA was prepared using RNeasy kit (QIAGEN). The RNA was DNase treated (Ambion), and first-strand cDNA synthesis was performed with Superscript (Invitrogen). Quantitative PCR (qPCR) was done on an Applied Biosystems 7300 real-time PCR system using FastStart Universal SYBR Green Master (Roche). Results were quantified using the $\Delta\Delta C_t$ method. PS1 levels were normalized to the housekeeping genes TATA-binding protein (TBP) or the ribosomal protein RPL27. Primers for PS1 spanned exons 4 and 5. The forward primer sequence is TGACTCTCTGCATGGTGGTGG. The reverse primer sequence is TCTCTGGCCCACAGTCTCGGT.

Aβ Measurements

NPCs were plated at a density of 5×10^5 in 12-well plates. Media was changed 24 hr after plating and replaced with 0.5 ml of NPC media + FGF. After 48 hr, media was harvested and stored at −80°C and protein was harvested for normalization purposes. Neurons were plated at density of 1.5×10^5 per 96-well in a 100 μl volume of glial conditioned media. Media was harvested from purified neurons after 2 weeks. Glial-conditioned medium was made by putting NPC media onto glia (Lonza) for 24 hr. Aβ from the media was measured with MSD Human (6E10) Abeta3-Plex Kits (Meso Scale Discovery). For experiments with γ-secretase inhibitor, all media was changed on day 3 and replaced with 100 μl of media either with compound E or DMSO (vehicle). All media was harvested on day 5. Compound E (EMD Chemicals) was used at

concentrations of 5 nM and 200 nM. Three to six independent measurements were made per line. Each NPC line was differentiated twice in independent experiments for purified neurons.

Gel Electrophoresis and Western Blot

Tissue culture lysates were prepared using radioimmunoprecipitation assay lysis buffer (Millipore) supplemented with protease (cocktail set I; Calbiochem) and phosphatase (Halt; Pierce) inhibitors. The bicinchoninic acid assay (Pierce) was used to estimate the protein content. Equal protein amounts were separated in MES buffer alongside Novex Sharp prestained markers (Invitrogen) on NUPAGE 4%–12% Bis-Tris precast gels (Invitrogen) and then transferred to polyvinylidene fluoride or nitrocellulose (0.45 μm pore size Immobilon; Millipore). Membranes were blocked in 5% BSA in tris-buffered saline with 0.1% Tween-20 or Odyssey Blocking Buffer (LI-COR Biosciences). Primary antibodies (presenilin 1 c-loop 1:1,000, Chemicon; presenilin 1 N-term 1:1,000, Santa Cruz; APP C terminus 1:1,000, Calbiochem; N-cadherin C terminus 1:1,000, BD Biosciences; nicastrin 1:1,000, Affinity BioReagents; actin C4 1:100,000, Chemicon; tubulin-alpha DM1A 1:50,000, Sigma) were prepared in 5% BSA. Fluorescent secondary antibodies (LI-COR Biosciences) were diluted 1:5,000. LI-COR Biosciences Odyssey infrared imager was used to measure pixel intensities of bands at detector settings set at the maximum or one-half unit below saturation. For each protein band, background-subtracted integrated intensity values were calculated using the Odyssey software. Given that absolute integrated intensity values vary for the same samples on different blots, samples within a blot were plotted relative to control, and these normalized values were used to average replicates from separate blots. To show protein bands in the conventional manner with dark bands on a light background, grayscale images were inverted in the figures. Horseradish peroxidase-conjugated secondary antibodies (Invitrogen) were diluted 1:5,000. Blots were developed using ECL Western Blotting Kit (Pierce).

Statistical Methods

All data were analyzed using GraphPad Prism Software (GraphPad). Statistical analysis comparing different genotypes was performed by Tukey's multiple comparison test. Drug responses were compared to controls by Dunnett's test.

SUPPLEMENTAL INFORMATION

Supplemental Information includes Supplemental Experimental Procedures and two figures and can be found with this article online at http://dx.doi.org/10.1016/j.celrep.2013.10.018.

REFERENCES

Ashe, K.H., and Zahs, K.R. (2010). Probing the biology of Alzheimer's disease in mice. Neuron 66, 631–645.

Barnes, D.E., and Yaffe, K. (2011). The projected effect of risk factor reduction on Alzheimer's disease prevalence. Lancet Neurol. 10, 819–828.

Bentahir, M., Nyabi, O., Verhamme, J., Tolia, A., Horré, K., Wiltfang, J., Esselmann, H., and De Strooper, B. (2006). Presenilin clinical mutations can affect gamma-secretase activity by different mechanisms. J. Neurochem. 96, 732–742.

Buerger, K., Ewers, M., Pirttilä, T., Zinkowski, R., Alafuzoff, I., Teipel, S.J., DeBernardis, J., Kerkman, D., McCulloch, C., Soininen, H., and Hampel, H. (2006). CSF phosphorylated tau protein correlates with neocortical neurofibrillary pathology in Alzheimer's disease. Brain 129, 3035–3041.

Chambers, S.M., Fasano, C.A., Papapetrou, E.P., Tomishima, M., Sadelain, M., and Studer, L. (2009). Highly efficient neural conversion of human ES and iPS cells by dual inhibition of SMAD signaling. Nat. Biotechnol. 27, 275–280.

Chávez-Gutiérrez, L., Bammens, L., Benilova, I., Vandersteen, A., Benurwar, M., Borgers, M., Lismont, S., Zhou, L., Van Cleynenbreugel, S., Esselmann, H., et al. (2012). The mechanism of γ-Secretase dysfunction in familial Alzheimer disease. EMBO J. 31, 2261–2274.

Chen, F., Pruett-Miller, S.M., Huang, Y., Gjoka, M., Duda, K., Taunton, J., Collingwood, T.N., Frodin, M., and Davis, G.D. (2011). High-frequency genome editing using ssDNA oligonucleotides with zinc-finger nucleases. Nat. Methods 8, 753–755.

De Strooper, B., Saftig, P., Craessaerts, K., Vanderstichele, H., Guhde, G., Annaert, W., Von Figura, K., and Van Leuven, F. (1998). Deficiency of presenilin-1 inhibits the normal cleavage of amyloid precursor protein. Nature 391, 387–390.

De Strooper, B., Annaert, W., Cupers, P., Saftig, P., Craessaerts, K., Mumm, J.S., Schroeter, E.H., Schrijvers, V., Wolfe, M.S., Ray, W.J., et al. (1999). A presenilin-1-dependent gamma-secretase-like protease mediates release of Notch intracellular domain. Nature 398, 518–522.

Ding, Q., Lee, Y.K., Schaefer, E.A., Peters, D.T., Veres, A., Kim, K., Kuperwasser, N., Motola, D.L., Meissner, T.B., Hendriks, W.T., et al. (2013). A TALEN genome-editing system for generating human stem cell-based disease models. Cell Stem Cell 12, 238–251.

Edbauer, D., Winkler, E., Regula, J.T., Pesold, B., Steiner, H., and Haass, C. (2003). Reconstitution of gamma-secretase activity. Nat. Cell Biol. 5, 486–488.

Extance, A. (2010). Alzheimer's failure raises questions about disease-modifying strategies. Nat. Rev. Drug Discov. 9, 749–751.

Games, D., Adams, D., Alessandrini, R., Barbour, R., Berthelette, P., Blackwell, C., Carr, T., Clemens, J., Donaldson, T., Gillespie, F., et al. (1995). Alzheimer-type neuropathology in transgenic mice overexpressing V717F beta-amyloid precursor protein. Nature 373, 523–527.

Gore, A., Li, Z., Fung, H.L., Young, J.E., Agarwal, S., Antosiewicz-Bourget, J., Canto, I., Giorgetti, A., Israel, M.A., Kiskinis, E., et al. (2011). Somatic coding mutations in human induced pluripotent stem cells. Nature 471, 63–67.

Heilig, E.A., Xia, W., Shen, J., and Kelleher, R.J., 3rd. (2010). A presenilin-1 mutation identified in familial Alzheimer disease with cotton wool plaques causes a nearly complete loss of gamma-secretase activity. J. Biol. Chem. 285, 22350–22359.

Hockemeyer, D., Wang, H., Kiani, S., Lai, C.S., Gao, Q., Cassady, J.P., Cost, G.J., Zhang, L., Santiago, Y., Miller, J.C., et al. (2011). Genetic engineering of human pluripotent cells using TALE nucleases. Nat. Biotechnol. 29, 731–734.

Hussein, S.M., Batada, N.N., Vuoristo, S., Ching, R.W., Autio, R., Närvä, E., Ng, S., Sourour, M., Hämäläinen, R., Olsson, C., et al. (2011). Copy number variation and selection during reprogramming to pluripotency. Nature 471, 58–62.

Israel, M.A., Yuan, S.H., Bardy, C., Reyna, S.M., Mu, Y., Herrera, C., Hefferan, M.P., Van Gorp, S., Nazor, K.L., Boscolo, F.S., et al. (2012). Probing sporadic and familial Alzheimer's disease using induced pluripotent stem cells. Nature 482, 216–220.

Jiang, Y., Mullaney, K.A., Peterhoff, C.M., Che, S., Schmidt, S.D., Boyer-Boiteau, A., Ginsberg, S.D., Cataldo, A.M., Mathews, P.M., and Nixon, R.A. (2010). Alzheimer's-related endosome dysfunction in Down syndrome is Abeta-independent but requires APP and is reversed by BACE-1 inhibition. Proc. Natl. Acad. Sci. USA 107, 1630–1635.

Killick, R., Pollard, C.C., Asuni, A.A., Mudher, A.K., Richardson, J.C., Rupniak, H.T., Sheppard, P.W., Varndell, I.M., Brion, J.P., Levey, A.I., et al. (2001). Presenilin 1 independently regulates beta-catenin stability and transcriptional activity. J. Biol. Chem. 276, 48554–48561.

Koch, P., Tamboli, I.Y., Mertens, J., Wunderlich, P., Ladewig, J., Stüber, K., Esselmann, H., Wiltfang, J., Brüstle, O., and Walter, J. (2012). Presenilin-1 L166P mutant human pluripotent stem cell-derived neurons exhibit partial loss of γ-secretase activity in endogenous amyloid-β generation. Am. J. Pathol. 180, 2404–2416.

Kumar-Singh, S., Theuns, J., Van Broeck, B., Pirici, D., Vennekens, K., Corsmit, E., Cruts, M., Dermaut, B., Wang, R., and Van Broeckhoven, C. (2006). Mean age-of-onset of familial alzheimer disease caused by presenilin mutations correlates with both increased Abeta42 and decreased Abeta40. Hum. Mutat. 27, 686–695.

Lee, J.H., Yu, W.H., Kumar, A., Lee, S., Mohan, P.S., Peterhoff, C.M., Wolfe, D.M., Martinez-Vicente, M., Massey, A.C., Sovak, G., et al. (2010). Lysosomal proteolysis and autophagy require presenilin 1 and are disrupted by Alzheimer-related PS1 mutations. Cell 141, 1146–1158.

Leem, J.Y., Vijayan, S., Han, P., Cai, D., Machura, M., Lopes, K.O., Veselits, M.L., Xu, H., and Thinakaran, G. (2002). Presenilin 1 is required for maturation and cell surface accumulation of nicastrin. J. Biol. Chem. 277, 19236–19240.

Levy, S., Sutton, G., Ng, P.C., Feuk, L., Halpern, A.L., Walenz, B.P., Axelrod, N., Huang, J., Kirkness, E.F., Denisov, G., et al. (2007). The diploid genome sequence of an individual human. PLoS Biol. 5, e254.

Lister, R., Pelizzola, M., Kida, Y.S., Hawkins, R.D., Nery, J.R., Hon, G., Antosiewicz-Bourget, J., O'Malley, R., Castanon, R., Klugman, S., et al. (2011). Hotspots of aberrant epigenomic reprogramming in human induced pluripotent stem cells. Nature 471, 68–73.

Mali, P., Yang, L., Esvelt, K.M., Aach, J., Guell, M., DiCarlo, J.E., Norville, J.E., and Church, G.M. (2013). RNA-guided human genome engineering via Cas9. Science 339, 823–826.

Miller, J.C., Tan, S., Qiao, G., Barlow, K.A., Wang, J., Xia, D.F., Meng, X., Paschon, D.E., Leung, E., Hinkley, S.J., et al. (2011). A TALE nuclease architecture for efficient genome editing. Nat. Biotechnol. 29, 143–148.

Naruse, S., Thinakaran, G., Luo, J.J., Kusiak, J.W., Tomita, T., Iwatsubo, T., Qian, X., Ginty, D.D., Price, D.L., Borchelt, D.R., et al. (1998). Effects of PS1 deficiency on membrane protein trafficking in neurons. Neuron 21, 1213–1221.

Opar, A. (2008). Mixed results for disease-modification strategies for Alzheimer's disease. Nat. Rev. Drug Discov. 7, 717–718.

Perez-Tur, J., Froelich, S., Prihar, G., Crook, R., Baker, M., Duff, K., Wragg, M., Busfield, F., Lendon, C., Clark, R.F., et al. (1995). A mutation in Alzheimer's disease destroying a splice acceptor site in the presenilin-1 gene. Neuroreport 7, 297–301.

Qiang, L., Fujita, R., Yamashita, T., Angulo, S., Rhinn, H., Rhee, D., Doege, C., Chau, L., Aubry, L., Vanti, W.B., et al. (2011). Directed conversion of Alzheimer's disease patient skin fibroblasts into functional neurons. Cell 146, 359–371.

Radde, R., Duma, C., Goedert, M., and Jucker, M. (2008). The value of incomplete mouse models of Alzheimer's disease. Eur. J. Nucl. Med. Mol. Imaging 35 (Suppl 1), S70–S74.

Refolo, L.M., Eckman, C., Prada, C.M., Yager, D., Sambamurti, K., Mehta, N., Hardy, J., and Younkin, S.G. (1999). Antisense-induced reduction of presenilin 1 expression selectively increases the production of amyloid beta42 in transfected cells. J. Neurochem. 73, 2383–2388.

Rodrigues, E.M., Weissmiller, A.M., and Goldstein, L.S.B. (2012). Enhanced β-secretase processing alters APP axonal transport and leads to axonal defects. Hum. Mol. Genet. 21, 4587–4601.

Rovelet-Lecrux, A., Hannequin, D., Raux, G., Le Meur, N., Laquerrière, A., Vital, A., Dumanchin, C., Feuillette, S., Brice, A., Vercelletto, M., et al. (2006). APP locus duplication causes autosomal dominant early-onset Alzheimer disease with cerebral amyloid angiopathy. Nat. Genet. 38, 24–26.

Sander, J.D., Cade, L., Khayter, C., Reyon, D., Peterson, R.T., Joung, J.K., and Yeh, J.R. (2011). Targeted gene disruption in somatic zebrafish cells using engineered TALENs. Nat. Biotechnol. *29*, 697–698.

Sato, T., Dohmae, N., Qi, Y., Kakuda, N., Misonou, H., Mitsumori, R., Maruyama, H., Koo, E.H., Haass, C., Takio, K., et al. (2003). Potential link between amyloid beta-protein 42 and C-terminal fragment gamma 49-99 of beta-amyloid precursor protein. J. Biol. Chem. *278*, 24294–24301.

Saura, C.A., Choi, S.Y., Beglopoulos, V., Malkani, S., Zhang, D., Shankaranarayana Rao, B.S., Chattarji, S., Kelleher, R.J., 3rd, Kandel, E.R., Duff, K., et al. (2004). Loss of presenilin function causes impairments of memory and synaptic plasticity followed by age-dependent neurodegeneration. Neuron *42*, 23–36.

Scheuner, D., Eckman, C., Jensen, M., Song, X., Citron, M., Suzuki, N., Bird, T.D., Hardy, J., Hutton, M., Kukull, W., et al. (1996). Secreted amyloid β-protein similar to that in the senile plaques of Alzheimer's disease is increased *in vivo* by the presenilin 1 and 2 and APP mutations linked to familial Alzheimer's disease. Nat. Med. *2*, 864–870.

Shen, J., and Kelleher, R.J., 3rd. (2007). The presenilin hypothesis of Alzheimer's disease: evidence for a loss-of-function pathogenic mechanism. Proc. Natl. Acad. Sci. USA *104*, 403–409.

Shen, J., Bronson, R.T., Chen, D.F., Xia, W., Selkoe, D.J., and Tonegawa, S. (1997). Skeletal and CNS defects in Presenilin-1-deficient mice. Cell *89*, 629–639.

Shepherd, C.E., Gregory, G.C., Vickers, J.C., Brooks, W.S., Kwok, J.B.J., Schofield, P.R., Kril, J.J., and Halliday, G.M. (2004). Positional effects of presenilin-1 mutations on tau phosphorylation in cortical plaques. Neurobiol. Dis. *15*, 115–119.

Shi, Y., Kirwan, P., Smith, J., MacLean, G., Orkin, S.H., and Livesey, F.J. (2012). A human stem cell model of early Alzheimer's disease pathology in Down syndrome. Sci. Transl. Med. *4*, 24ra29.

Soldner, F., Laganière, J., Cheng, A.W., Hockemeyer, D., Gao, Q., Alagappan, R., Khurana, V., Golbe, L.I., Myers, R.H., Lindquist, S., et al. (2011). Generation of isogenic pluripotent stem cells differing exclusively at two early onset Parkinson point mutations. Cell *146*, 318–331.

Takahashi, K., Tanabe, K., Ohnuki, M., Narita, M., Ichisaka, T., Tomoda, K., and Yamanaka, S. (2007). Induction of pluripotent stem cells from adult human fibroblasts by defined factors. Cell *131*, 861–872.

Tanzi, R.E., and Bertram, L. (2005). Twenty years of the Alzheimer's disease amyloid hypothesis: a genetic perspective. Cell *120*, 545–555.

Thinakaran, G., Borchelt, D.R., Lee, M.K., Slunt, H.H., Spitzer, L., Kim, G., Ratovitsky, T., Davenport, F., Nordstedt, C., Seeger, M., et al. (1996). Endoproteolysis of presenilin 1 and accumulation of processed derivatives in vivo. Neuron *17*, 181–190.

Wolfe, D.M., Lee, J.H., Kumar, A., Lee, S., Orenstein, S.J., and Nixon, R.A. (2013). Autophagy failure in Alzheimer's disease and the role of defective lysosomal acidification. Eur. J. Neurosci. *37*, 1949–1961.

Yagi, T., Ito, D., Okada, Y., Akamatsu, W., Nihei, Y., Yoshizaki, T., Yamanaka, S., Okano, H., and Suzuki, N. (2011). Modeling familial Alzheimer's disease with induced pluripotent stem cells. Hum. Mol. Genet. *20*, 4530–4539.

Yuan, S.H., Martin, J., Elia, J., Flippin, J., Paramban, R.I., Hefferan, M.P., Vidal, J.G., Mu, Y., Killian, R.L., Israel, M.A., et al. (2011). Cell-surface marker signatures for the isolation of neural stem cells, glia and neurons derived from human pluripotent stem cells. PLoS ONE *6*, e17540.